Kinematics-Based Control of an Inflatable Soft Wearable Robot for Assisting the Shoulder of Industrial Workers

Yu Meng Zhou, Cameron Hohimer, Tommaso Proietti, Ciarán Tomás O'Neill, and Conor J. Walsh

***Abstract*—Recent developments in soft active wearable robots can be used for upper extremity injury prevention for healthy industrial workers with better comfort than rigid systems, but there has not been control strategy proposals for such use cases. In this letter, we introduce a kinematics-based controller for an inflatable soft wearable robot that provides assistance to the shoulder quickly and accurately when needed during industrial use cases. Our approach is to use a state machine to classify user intent using shoulder and trunk kinematics estimated with body-worn inertial measurement units. We recruited eight participants to perform various tasks common in the workplace and assessed the controller's intent classification accuracy and response times, by using the users' reactions to cues as their ground truth intentions. On average, we found that the kinematics controller had 99% classification accuracy, and responded 0.8 seconds after the users reacted to the cue to begin work and 0.5 seconds after the users reacted to a cue to stop the task. In addition, we implemented an EMG-based controller for comparison, with state transitions determined by EMG-based thresholds instead of kinematics. Compared to the EMG controller, the kinematics controller required similar time to detect the users' intentions to stop overhead work but an additional 0.17 seconds on average for detecting users' intentions to begin. Although slightly slower, the kinematics controller still provided support prior to users' work initiations. We also implemented an online adaptive tuning algorithm for the kinematics controller to speed up response time while ensuring accuracy during offset transitions. This research paves the way for a further study of kinematics-based controller in a mobile system in real work environments.**

***Index Terms*—Intention recognition, soft robot applications, wearable robotics.**

I. Introduction

SHOULDER injuries from strenuous overhead work, common on industry production lines, require long recovery times. In 2018, there were 68 070 cases of workplace shoulder injuries resulting in a median of 27 days away from work per case [1]. The repetitive and prolonged overhead postures required in the industrial setting are major contributors of shoulder injuries, fatigue, and discomfort [2]. Existing injury prevention efforts, such as limiting task duty cycles and introducing more task rotations, can be expensive to implement and challenging to enforce. More recently, upper extremity wearable robots have been considered as an effective injury prevention method as they allow load reduction for joints such as the shoulder, neck and upper back [3].

Currently, the development of wearable robots as personal protective equipment is growing in both research and commercial development. These devices can be divided into two categories based on their architecture: rigid and soft. Commercially available exoskeletons such as the Ekso Bionics Evo and the Levitate Airframe, are rigid and passive by design. These elegantly designed systems provide support by mechanically redistributing load using spring clutch mechanisms, and they do not require power or control electronics. Recent studies using these rigid passive exoskeletons have shown promising results such as their transparency for horizontal precision tasks [4] and their ability to reduce anterior deltoid muscle activation for participants performing overhead pointing tasks [5]. However, the rigid form factor of these commercial passive devices can result in some discomfort at loading points on the body and presents the risk of scratching delicate parts on the production line. Moreover, passive devices require antagonistic muscles to push against device to release support which can result in no net decrease of load on the body in some cases [6].

In contrast to rigid passive devices, there is also growing interest in soft active wearable robots for assisting single or multiple joints for the upper extremity. These devices have been primarily designed for medical purposes such as stroke rehabilitation. Examples in this category include cable-driven devices for elbow gravity compensation [7], [8], inflatable pneumatic devices for assisting shoulder disabilities [9], [10], and a shoulder, elbow, and wrist cable-driven device for stroke rehabilitation [11]. Compared to rigid exoskeletons, these soft devices offer the promise of limited mass on the limb, better comfort, and less kinematic restriction from joint misalignment. A benefit of soft wearable robots is that when powered off they can be transparent to the wearer and not restrict their movements. However, as a result they require active control to determine when to apply assistance.

State of the art controller development for these devices include admittance controllers with cable displacement models for

Manuscript received October 15, 2020; accepted February 14, 2021. Date of publication February 23, 2021; date of current version March 11, 2021. This letter was recommended for publication by Associate Editor Ki-Uk Kyung and Editor Jee-Hwan Ryu upon evaluation of the reviewers' comments. This work was supported by the Tata-Harvard Alliance, National Science Foundation EFRI Award (1830896). *(Corresponding author: Conor James Walsh.)*

The authors are with the John A. Paulson School of Engineering and Applied Sciences, Harvard University, Cambridge, MA 02138 USA (e-mail: yumengzhou@seas.harvard.edu; chohimer@g.harvard.edu; tproietti@g.harvard.edu; ciaranoneill@g.harvard.edu; walsh@seas.harvard.edu).

Digital Object Identifier 10.1109/LRA.2021.3061365

gravity compensation [12] and biomimetic controllers for bilateral training for stroke rehabilitation [11]. Both these controllers were developed for medical applications, but the requirements for interacting with healthy individuals are quite different with more emphasis on intention detection. In order to further the use of soft wearable robots as an injury prevention tool, we require new control approaches appropriate for healthy individuals. In the industrial use case, an intuitive control strategy for using a soft wearable robot should detect user's intention quickly and accurately, and apply assistance only when required. This requirement has not been fulfilled by existing work, and in this letter we propose a control strategy based on user kinematics.

For wearable robot controls, kinematic sensing has been widely pursued in lower limb exoskeleton control either by directly applying joint kinematics [13] or using timing-based events [14], but not as often for upper extremity systems. EMG-based intention detection, although laborious in sensor donning, has shown potential for upper extremity applications in prior research, including classification of tasks and movement directions with extracted EMG features [15], [16], linking intentions through estimated joint torques from kinematics and EMG [17], [18], and thresholding based on normalized EMG to trigger when assistance is required [19], [20].

In this letter, we present a kinematics-based controller for a soft wearable robot designed to assist the shoulder joint of healthy industrial workers. Our soft inflatable shoulder robot has been previously targeted towards medical applications [9], and our focus here is the controller design for industrial applications for healthy users with a similar version of the device. The controller is intuitive to use, needs minimal calibration after donning, and adapts its offset velocity threshold to best follow user intention during use. We conducted human subject experiments with 8 healthy participants simulating common functional industrial tasks to evaluate controller performance in terms of classification accuracy and response timing. Visual and audio cues were provided to participants and acted as the ground truth of user intentions. The controller response times were measured from users' reaction times to cues. In addition, we compared the kinematics controller to a similar state machine controller using EMG sensing and observed the response time differences between the two controllers.

II. Device and Components

The design of our inflatable shoulder support robot for industrial applications built off our previously published work [9]. The device consisted of an athletic shirt with a non-extensible harness and pneumatic textile actuator (Fig. 1(a). The actuator was designed to support the arm against gravity and its bifurcated shape cradles the arm for more stability. To estimate shoulder elevation angles, inertial measurement units (IMUs) (Xsens MTi-3 series) were attached to the back of the shirt and on each sleeve (Fig. 1(a).

During this early stage research, we leveraged a tethered offboard actuation system (Fig. 1(b)), that provided a flexible development platform before we design a future mobile system. The actuation platform included a pressure regulator (SMC,

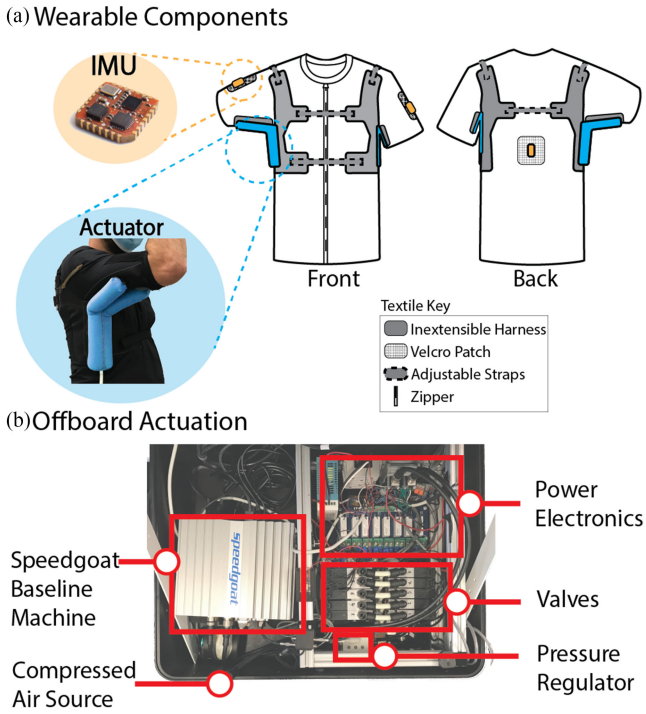

Fig. 1. Components of (a) the wearable device with actuator and sensors close-ups images (IMU image from Xsens documentation), and (b) developmental offboard actuation system.

Japan), 3/2 way direct operation valves (Humphery, USA), and pressure sensors (Honeywell, USA), and was controlled using Simulink Realtime (Mathworks, USA) with a Speedgoat baseline machine (Speedgoat, Switzerland). The Speedgoat machine used IO601 for CAN communication with the IMUs.

III. Controller Design

Our major requirements for the controller are to (1) support repetitive and prolonged overhead work at high shoulder elevation angles; (2) accurately classify user intention and rapidly follow changes in intention; (3) not impede other motions by both leveraging its soft architecture and high classification accuracy; and (4) need minimal calibration after donning to allow quick use. Based on above requirements, we designed a kinematics-based controller with an adaptive feature to adjust a key threshold in real time, and we implemented a similar state machine controller using EMG signals for comparison through experimental data on their relative performances on users.

Both controllers used state machines to transition between the *inflated* state which provided assistance at constant actuator pressure ($P = P_{act}$), and the *deflated* state which was transparent and nonrestrictive to user motion ($P = 0$). We set a different P_{act} for each user, defined as the minimum pressure required to support the user's arm angle above a rest angle of 70°. The range of P_{act} was between 10 psi and 16 psi. The controllers also used a common actuator state detection algorithm to allow state transitions only when actuators were fully *inflated* or *deflated*.

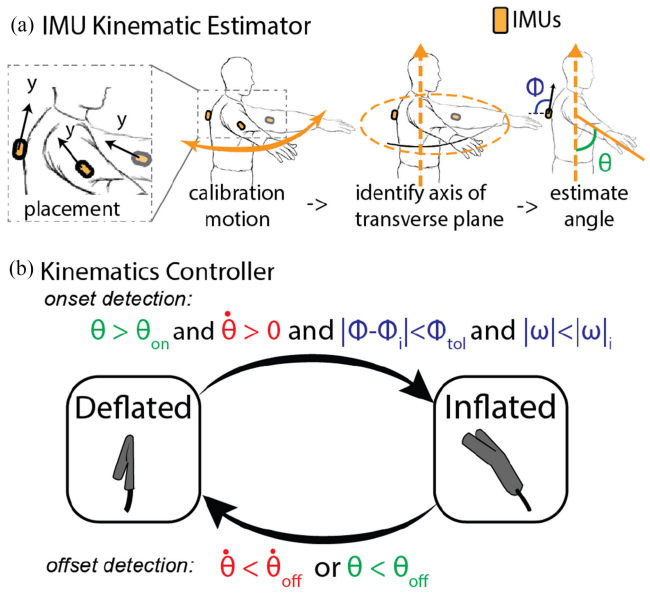

Fig. 2. (a) IMU-based shoulder elevation angle estimation with sensor placement, calibration procedure and working principle. (b) Kinematics controller state machine with onset and offset detection logic. θ is the shoulder elevation angle, $\dot{\theta}$ is the elevation angular velocity, ϕ is the trunk inclination angle (roll in our case as y axis of trunk IMU was along the spine), and $|\omega|$ is the norm of trunk IMU gyroscope.

A. Kinematics Controller

1) IMU Kinematic Estimator: The kinematics controller used an IMU estimator to determine shoulder elevation angle and angular velocity. The arm and trunk IMUs were oriented with their y axes aligned along the length of the humerus and spine respectively (Fig. 2(a). A simple calibration routine, in which users performed horizontal flexion and extension, was used to identify and calibrate the vertical axis normal to the transverse plane in the frame of the trunk IMU. From the trunk IMU frame, the elevation angle was estimated as the angle difference between the the arm IMU y axis and calibrated vertical axis (Fig. 2(a). To obtain elevation velocity, we used finite difference method with smoothing window of 0.1 s.

2) Controller State Machine: The transitions between the controller states were determined by logical statements based on the shoulder and trunk kinematics (Fig. 2(b)). In particular, the state machine transitioned from *deflated* to *inflated* when the: *(1)* arm elevation angle (θ) was greater than the onset angle (θ_{on}); *(2)* the arm angular velocity ($\dot{\theta}$) was positive; *(3)* the trunk inclination angle (ϕ) was within a tolerance threshold (ϕ_{tol}) of the initial trunk inclination angle (ϕ_i) found during initial calibration; and *(4)* the trunk IMU gyroscope norm ($|\omega|$) was below the maximum reading during initial calibration. The state machine transitioned from *inflated* to *deflated* when either: *(1)* the arm elevation angle dropped below the offset angle(θ_{off}); or *(2)* the elevation velocity crossed the offset velocity ($\dot{\theta}_{off}$) threshold. During initial controller calibration, users performed a series of overhead reaching motions consistent with overhead work, to calibrate state machine parameters including ϕ_i, $|\omega|_i$.

The rationale behind the specific state machine thresholds and whether they were fixed, calibrated or adaptive during use, was based on the use case of overhead work. For this industrial application, overhead work is often performed with the workers' trunks steady and upright, hence we obtained ϕ_i and $|\omega|_i$ from the initial calibration motion, and set $\phi_{tol} = 20°$. Because injuries often occur during prolonged elevated manipulation of tools, we set a fixed onset angle of $\theta_{on} = 70°$, which corresponds to typical hand/tool positions.

For the offset angle, we chose an angle lower than the onset angle, in order to give a range of angles at which the user can work with support from the device. Based on initial experimentation, we chose a fixed offset angle of $\theta_{off} = 60°$. In addition to using the offset angle, the offset velocity threshold crossing can also trigger the state machine offset transition from *inflated* to *deflated*. In fact, by using the offset velocity threshold rather than the offset angle, less effort from the user is required to push against the device (i.e. a smaller angular displacement is needed), providing greater comfort and faster response. Given this, we designed the offset velocity threshold parameter to be adaptable in real time. The initial offset velocity threshold was set during the calibration motions (same as motions for setting ϕ_i, $|\omega|_i$), as the minimum velocity reached one second before the offset angle crossing. In the following section, we describe the specific scenarios upon which the controller would adapt its offset velocity.

3) Offset Velocity Adaptation: Fig. 3 describes whether and how the offset velocity should adapt in three different scenarios. In Fig. 3(a), the offset velocity crossing was detected followed by the offset angle threshold crossing. This order of events confirmed that the user indeed intended to lower their arm, and the state machine detected this offset intent earlier than the offset angle threshold crossing. This is the ideal scenario for fast offset and accurate intent, and the velocity offset does not need to be adapted. The initial calibrated offset velocity was set to encourage this scenario.

In Fig. 3(b), the offset velocity would be *increased* as the threshold would only be crossed after detecting the angle threshold crossing. In this scenario, the controller responded too slow and the velocity threshold was set too low for this particular motion, and it is adjusted for the next overhead work cycle for faster and more comfortable offset transition.

In Fig. 3(c), the offset velocity would be *decreased* as the offset velocity threshold was met but not followed by offset angle crossing. This suggested that the user was performing some motion with downward velocity during overhead work without intending to lower their arms entirely. The controller would first mis-classify in this situation, however, since the elevation angle quickly increased above the onset angle after deflation, the controller re-inflated the device to continue to provide support. In the next cycle, the offset velocity threshold would decrease to avoid this mis-deflation.

In scenarios *B* and *C*, the offset velocity adapted as

$$\dot{\theta}_{off} = \dot{\theta}_{off} + K(\dot{\theta}_m - \dot{\theta}_{off}) \tag{1}$$

where $\dot{\theta}_m$ is minimum velocity prior to deflation or inflation in scenarios B and C respectively. K is the gain to set the rate of adaptation, for which we used $K = 0.1$. As we designed

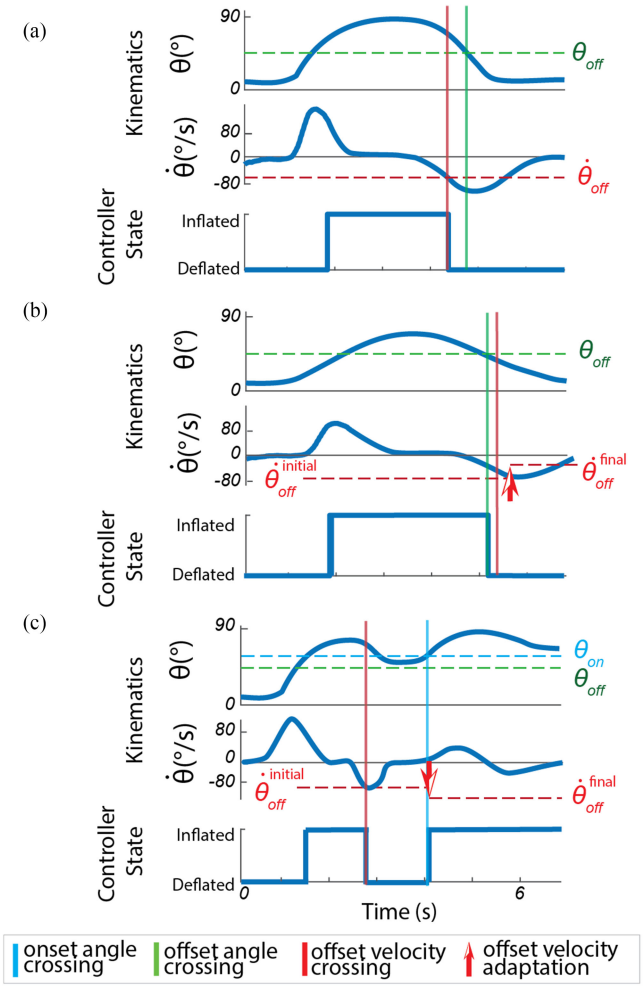

Fig. 3. Offset velocity adaptation showing 3 scenarios: (a) the sequence of velocity threshold crossing followed by angle threshold crossing are detected and the threshold does not need to changed, (b) the velocity threshold increases after the state transitions to deflated without detecting offset velocity threshold crossing, and (c) the offset velocity decreases after the controller mis-deflated (and quickly inflated) during motion with high velocity.

controller to react quickly and accurately, the adaptation occurred after each offset transition if scenarios *B* or *C* were detected.

B. EMG Controller

To compare with our kinematics controller, we developed a modified version of the state machine controller with EMG signals used to determine state transitions. We recognize that the state-of-the-art EMG intent detection include more sophistication, but for a practical system with fast calibration and minimal training data, we chose to first compare with a simple threshold-based controller to evaluate how the state machine would perform with this commonly used sensor. In prior research, thresholds using EMG normalized to maximum voluntary contraction (MVC) had been used to distinguish between assistance and power off modes of wearable devices [19], [20]. We took a similar approach of thresholding upon normalized EMG and combined with observed biomechanical patterns of

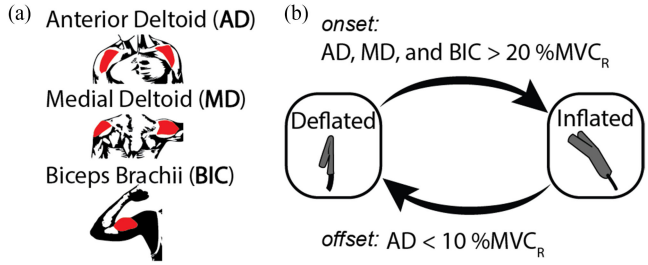

Fig. 4. EMG controller state machine highlighting (a) the muscle groups sensed and (b) the state machine transition conditions for onset and offset detection.

overhead motions. As overhead reach involves combined shoulder and elbow motion, we used anterior deltoid (AD), middle deltoid (MD) and bicep (BIC) as the muscle groups for EMG control (Fig. 4(a). For the industrial application, as different tasks require different relative activation to MVC, the EMG threshold we chose was based on EMG normalized to maximum contraction during the overhead reach reference motion (MVC_R) (same motion as kinematics controller calibration). As shown in Fig. 4(b), we used a threshold of 20% MVC_R for all AD, MD and BIC as onset detection to transition from *deflated* to *inflated* state. The offset detection used the relaxation of AD, the primary muscle responsible for shoulder forward flexion to transition from *inflated* to *deflated* state. This AD relaxation indicated the user's desire to lower their arm and was also correlated with when they stopped holding their tool steadily. We used $< 10\%$ MVC_R to detect AD relaxation and offset transition.

Our real-time EMG signals were collected at 1000 Hz, passed through a 4th order high pass filter with cutoff frequency of 20 Hz, rectified, and then applied a 4th order low pass filter at 10 Hz. The filtered signals were smoothed using a 2 s moving average window for more robust detection of steady activation.

IV. Experimental Method

We conducted a study with human subject participants aimed to: *(1)* assess the kinematics controller's classification performance in terms of response time and accuracy; *(2)* demonstrate that the controller can work with users in a realistic overhead task; and *(3)* compare the kinematics controller with the EMG controller from timing and accuracy data and sample user preference.

Under the Harvard University Institutional Review Board protocol IRB19-1321, we recruited 8 healthy subjects (29.63 ± 4.09 years old, 2 female and 6 male) to complete three experiments to assess the controller in a variety of simulated industrial tasks. Our objective for the system is to provide to provide bilateral support, but for this study we tested all participants with unilateral actuation on their dominant side as the control algorithm would be the same on both sides. The tasks ranged from consistent motions in structured environments, to motions at various working regions with dynamic transition movements (Fig. 5(a), (b)).

Experiment 1 focused on evaluating controller performance in a structured environment where participants were provided

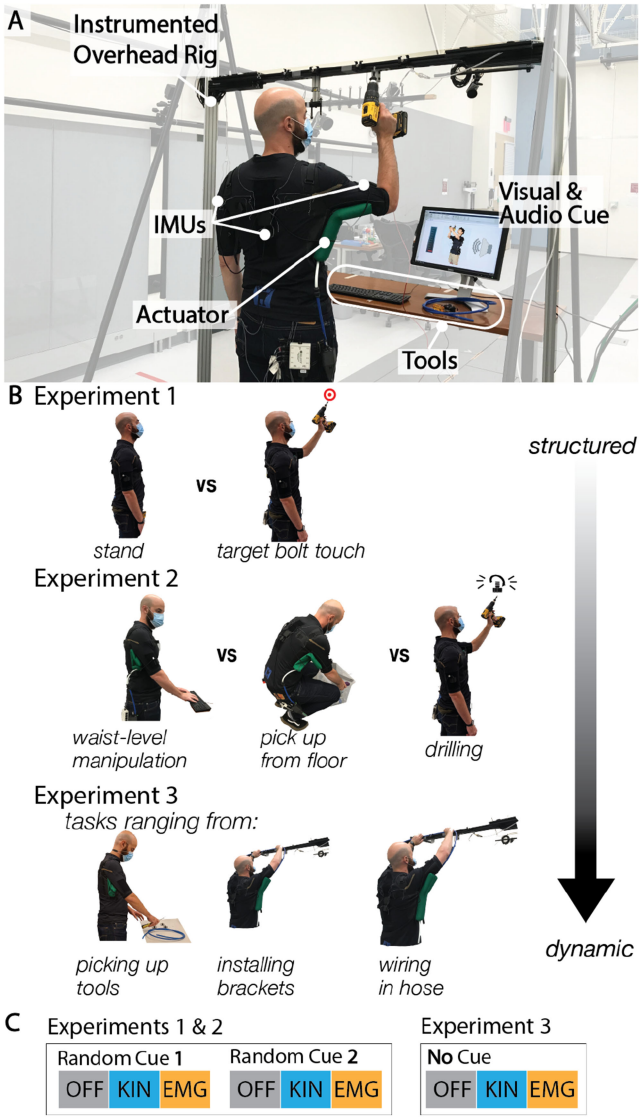

Fig. 5. (a) Human subject experiment photo showing subject wearing device performing cued tasks with provided tools. (b) Specific tasks from each experiment with labeled images. (c) Illustrated order of trials and their corresponding conditions – powered off (*OFF*), kinematics controller (*KIN*), and EMG controller (*EMG*).

visual and audio cues to prompt them to either stand still or to use a hand drill to touch and maintain contact with a target bolt. The cues acted as a reference for determining classification accuracy, and the user reaction times to the cues acted as a reference for controller state transition timing. The overhead test rig was also instrumented to detect when the participants made contact with the target bolt. The random cues were generated for $16 - 20$ target touches of random lengths for a total duration of 3 minutes per trial. The total number of cues per user can be slightly variable depending on the randomly generated length per cue.

We used the user reaction times to the given cues as the reference for evaluating controller response time in all trials. To quantify the user reaction time, we used the mean time at which the arm gyroscope norm exceeded its baseline noise level during each trial. The gyroscope signals are part of the raw IMU outputs, and we used the noise quantity documented in its datasheet. Using the gyroscope to quantify human reaction time has been shown in past work such as [21], who additionally showed gyroscope methods are faster than methods using accelerator or magnetometer. The reaction time was calculated for all trials, and we measured the controller response times starting from these reaction times for each participant.

In *experiment 2*, we prompted the users with visual and audio cues to simulate work in three common work regions: overhead, floor, and waist level. For the overhead work cue, we asked the participants to drill 2 in bolts in and out. For waist-level work, we provided tools and props, such as a keyboard, blocks, storage box, for users to type, stack and manipulate. For floor-level work, we asked participants to pick up objects such as boxes and safety cones on the ground. Among the three cues, the controller should only inflate the device and support the user during overhead drilling and stay deflated as the user performs other tasks. To evaluate accuracy, the cues acted as the ground truth for the user intention, and we considered a controller classification as accurate if the controller state matched the cued state (*inflated* for overhead drilling, and *deflated* for other tasks) for the entire duration of a task post initial user reaction. The cue profile was a randomly generated sequence and lengths of tasks, totaled up to 4 minutes per trial. The overhead drilling cues was set to be a minimum duration of 6 seconds and a maximum duration of 10 seconds. The waist-level and floor-level cues were set to be between 2 to 8 seconds. These specifications resulted in different numbers of total cues of each type per user.

For *experiment 1* and *2*, we tested each participant with two trials in the powered off condition (*OFF*), two trials with the kinematics controller (*KIN*) and two trials with the EMG controller (*EMG*). The condition order and corresponding cue profiles are described in Fig. 5(c).

In *experiment 3*, we asked the participants to perform a functional overhead hose wiring task. The task consisted of assembling of two T-slot hose clips, mounting of the clips on the overhead rig, and inserting a hose along the mounted clips. After a short pause, the users took down the hose and mounting clips in the reverse order. Users were asked to complete this task at a self-selected pace based on individual comfort level and not cued nor provided additional instructions during the duration of the task. Each participant performed the task once under the *OFF*, *KIN* and *EMG* conditions (Fig. 5(c)).

V. Results

In this section, we present and analyze the experimental data from both controllers.

A. Responsiveness

Fig. 6 shows the controller response times after initial user reaction during experiment 1. The differences among conditions were compared using a paired t-test followed by a post-hoc power analysis (required power $= 0.8$). We used p-values (p) as a probability measure that the observed result is unlikely or significant, with a smaller p-value suggesting a more significant

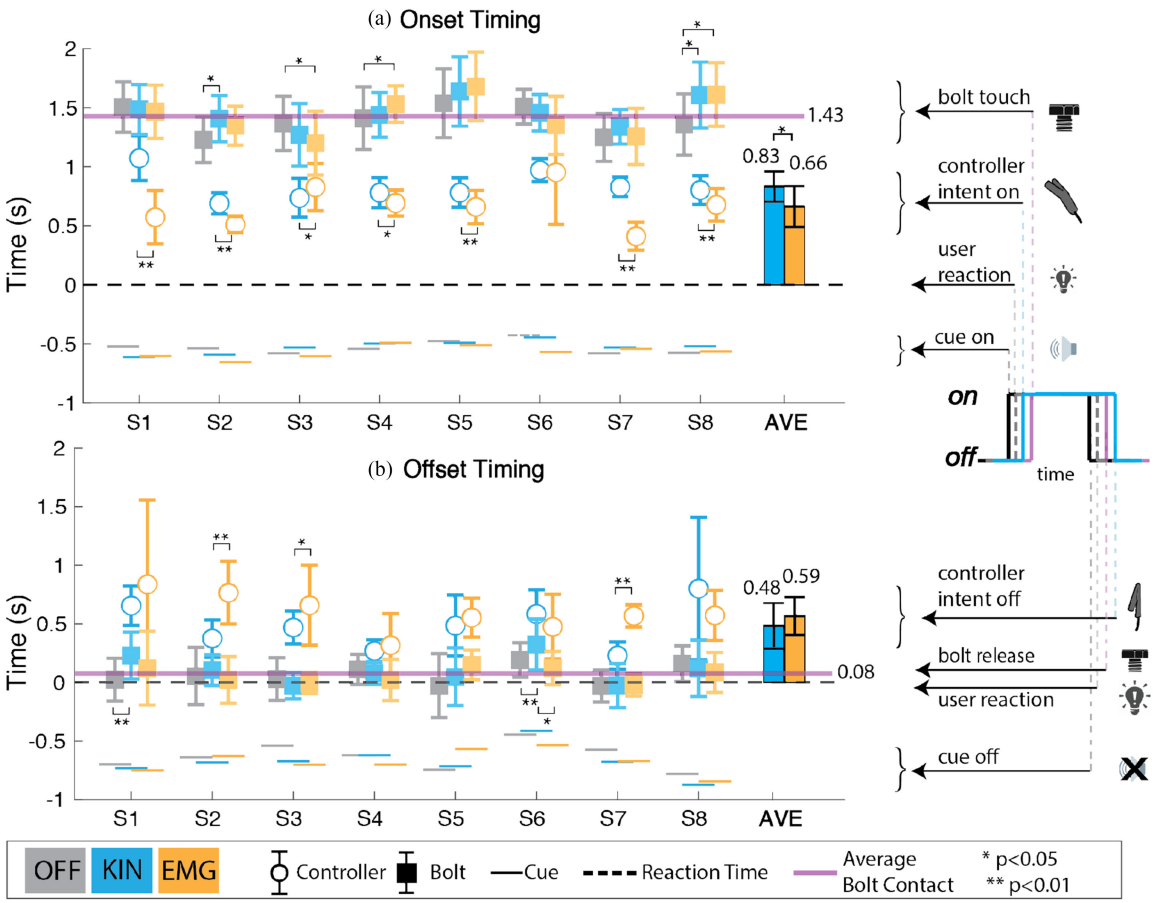

Fig. 6. Controller response timing data with (a) onset timing and (b) offset times of cue, human reaction, controller classification and bolt contact. Paired t-tests were conducted to calculate the statistical significance with a post-hoc power analysis (required power = 0.8). P-values (p) indicates the probability of observing the result under null hypothesis. Controller response for each individual and the averaged results are presented with the error bars indicating standard deviation. The bolt contact data is presented for each individual, with *purple* line indicating the average bolt contact across all conditions as there was minimal difference across averaged conditions.

difference between the conditions. We collected onset and offset timings of the subject reaction, controller classification, and tool contact. We the used reaction time in each trial as the reference timing or $t = 0$.

1) Onset: For the onset responses in Fig. 6(a), we saw both controllers classified intent on and triggered the inflation prior to the users making contact with the bolt. On average, the kinematics controller responded in 0.83 ± 0.13 seconds after human reaction, and the EMG controller responded in 0.66 ± 0.17 seconds after human reaction. The onset response of the EMG controller was faster than that of the kinematics controller on average ($p < 0.05$) by 0.17 seconds. For within subject comparison, the EMG controller responded faster than the kinematics controller for six participants ($p < 0.01$ for five and $p < 0.05$ for one). The difference between the controller responses was greatest for $S1$ and $S7$ with faster response in *EMG* condition by 0.5 seconds. For $S3$, the opposite was observed with the kinematics controller responding faster than the EMG controller ($p < 0.05$). For $S6$, there was no difference between the controller's onset response times. From this within subject comparison, we saw large variation in responses with the EMG controller being faster during onset for most participants.

2) Offset: For offset responses shown in Fig. 6(b), the users first reacted to the cue, released from the bolt, and then the controllers detected their offset intentions to deflated the device. On average, the kinematics controller responded in 0.48 ± 0.19 seconds after user reaction, and the EMG controller responded in 0.59 ± 0.16 seconds after user reaction. This difference was not significant on average, but the kinematics controller reacted faster than the EMG controller for three subjects ($p < 0.01$ for $S2$ and $S7$, $p < 0.05$ for $S3$) by at most 0.4 seconds.

3) Bolt Contact Time: In terms of time to touch and release from the target bolt, there was no significant difference in average bolt contact times with respect to user reaction time across all conditions. However, there were variations within subject experiences between *OFF* and controller (*KIN*, *EMG*) conditions. We observed both slower ($S2$ and $S8$ using *KIN*, $S4$ using *EMG*) and faster ($S3$ using *EMG*) bolt touch times with controller compared to *OFF* during onset (Fig. 6(a)), and slower bolt release times ($S1$ and $S6$ during *KIN*) compared to *OFF* (Fig. 6(b)). The maximum bolt contact time delays in *KIN* as compared to *OFF* condition for an individual subject were 0.25 seconds for onset and 0.21 seconds for offset, not long enough to cause consequential delays in work initiation.

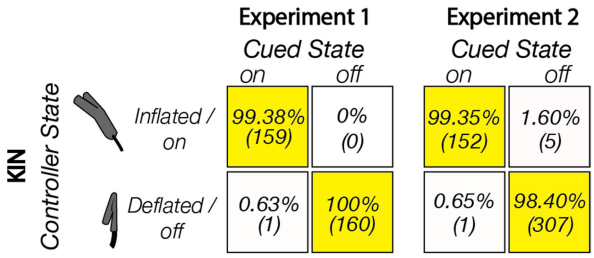

Fig. 7. Confusion matrix for kinematics controller intention classification for experiments 1 and 2.

Overall, we found both controllers were responsive (0.8 seconds for *KIN* and 0.7 seconds for *EMG*) after user reaction to cue, with the EMG controller being faster on the onset. Both controllers were able to assist prior to target touch and turned off quickly after bolt release. Additionally, the time to contact the target bolt during controller conditions was not different from that of *OFF* condition on average, indicating no delays to user tool operations caused by the controllers.

B. Accuracy

The overall accuracy rates of the kinematics controller considering all cues given were 99.7% in experiment 1 and 98.7% in experiment 2. Specifically, Fig. 7 shows the confusion matrix results for both experiments. In experiment 1, out a total of 160 cues from all participant data, there was 1 occurrence of mis-deflation during a bolt touch cue, and no occurrences of mis-inflation during standing cue. In experiment 2, out of a total of 153 cues for drilling, there was 1 occurrence of mis-deflation, and out of 312 other waist and floor-level task cues with no assistance needed, there were 5 occurrences of mis-inflations. Specifically, no intended inflations occurred during the floor-level tasks, and all 5 mis-triggers occurred during cues for waist-level work, some due to changes in shoulder elevation angle during simulated stacking task. The total numbers of cues for each type were slightly different due to the randomness of cue generation. The false positive rate was higher than the false negative rate during experiment 2, indicating the higher likelihood for the kinematics controller to provide undesired assistance than to remove support during overhead work. Although both are unfavourable behaviors, we feel avoiding false negatives to prevent sudden drops of tools and parts during overhead work is important for this application.

The EMG controller did not perform robustly, especially during experiment 2 (95.6% and 57.4% accuracy for experiments 1 and 2 respectively). Combined deltoid and bicep activation often occurred during waist and floor level tasks when the cued state was off and no assistance was required resulting in a high false positive rate. We observed that the EMG controller often mis-inflated during a short portion of the non-overhead tasks, and that there was large variations in responses among the participants.

C. Functional Task and User Preference

All participants completed the functional overhead wiring task with both controllers. As there were no reference cues, qualitative observations suggested both controllers were functional and matched the user intentions during the task.

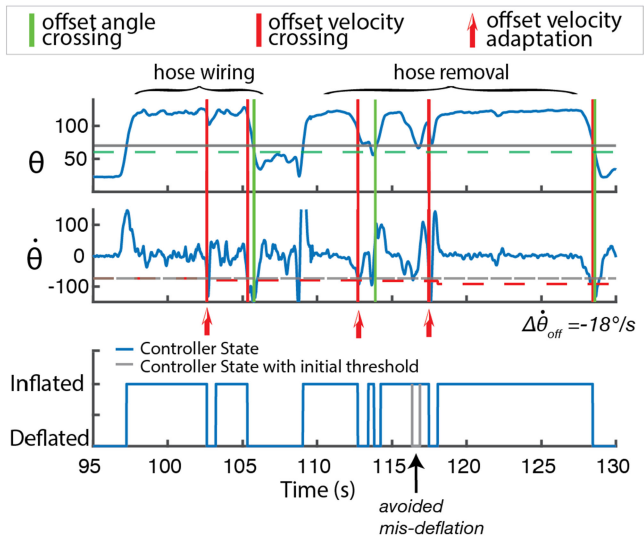

Fig. 8. An example of offset velocity adaptation (red arrows) during wiring task after the controller detected offset velocity crossing (red line) only and not offset angle crossing (green line). The controller using the initial offset velocity (controller state in grey solid line, and initial offset velocity in grey dashed line) would have experienced one extra unintended deflation.

After completing all experiments, participants provided verbal feedback of generally feeling helpful assistance and accurate assistance timing. Between the two controllers, 7 participants preferred the kinematics controller and 1 participant preferred the EMG controller. We observed the participant who preferred the EMG controller tended to lower their arms from the side (abduction), while the other participants lowered their arms from the front (forward flexion). A larger study may be needed to understand if this posture difference was related to controller preference and how the kinematic controller can better assist in abduction position.

D. Adaptive Offset Velocity Performance

During experiment 1, the kinematics controller adapted its offset velocity for six participants The adaptation occurred between 1 to 7 times per trial, and the adjustments were between $-3.8°/s$ and $5.5°/s$ from the initial offset velocity. The benefit of the adaptation as compared to no adaptation was shown in faster offsets responses, saving as much as 0.15 seconds between user reaction and controller offset detection. For experiment 2, the kinematics controller adapted the offset velocity for six participants in the range of $-12°/s$ and $1.5°/s$. The adaptation was skewed toward lower velocity thresholds as there was more dynamic movements in experiment 2. Without this adaptive threshold, more calibration time may be required to get representative reference motions of the various tasks to set a suitable offset velocity.

During experiment 3, velocity adaptation occurred for all participants. This experiment also involved fast movements and the offset velocities decreased as much as $19°/s$. Without these adaptations, the controller would have had more unintended deflations as illustrated in Fig. 8. For this participant, although

a few unintended deflations occurred during hose wiring and initial hose removal, the adaptive feature decreased the offset velocity each time (as in scenario C in Section III A) and as a result avoided one mis-deflations that would have happened if the threshold did not adapt. We see this deflation from the original controller (grey line) was unnecessary as the user continued to move at high elevation angles (70° to 110°) during this period of the task.

VI. Conclusion and Discussion

We hypothesized that a kinematics-based controller could be suitable for controlling soft wearable robots for healthy workers, and showed that our controller design had sufficient timing and accuracy performance. Through experimental data on their relative performances on users, we compared the kinematics controller to an EMG-based controller, a standard sensing method for wearable robot intention detection. With evaluation on 8 participants, we found that the kinematics controller had high intention detection accuracy of 99% in various work environments, onset response within 0.8 seconds and offset response within 0.5 seconds of user reaction on average. Compared to the EMG thresholding controller, the kinematics controller was slower by 0.17 seconds during onset intention detection. Considering the relative importance of requirements and trade-offs, we feel that a high intention detection accuracy with low false negative rate and an onset response within 1 s is sufficient for our target industrial use case, especially when the kinematics controller can provide assistance prior to the user's tool contacting the target. Our EMG controller implementation was limited, and we recognize that an alternative EMG-based approach, such as using machine learning with feature selection, could have improved accuracy. Regardless this comparison to a simple EMG state machine controller was useful in understanding the relative performance of the same controller type with different sensors. We found with a simple state machine controller structure, kinematics sensing was more robust.

We observed that the adaptive feature of our kinematics controller was useful in decreasing the controller response time during offset and reducing the number of unintended deflations during the dynamic wiring task. In future work, we would like to run longer experiments of repetitive functional tasks to test if the offset threshold would converge to after a certain duration with repeated movement patterns. This research paves the way for further study of a kinematics-based controller in an autonomous version of the system in real work environments.

References

[1] "TABLE R13. Number of nonfatal occupational injuries and illnesses involving days away from work by nature of injury or illness and selected parts of body affected by injury or illness, private industry," 2019. [Online]. Available: https://www.bls.gov/web/osh/cd_r13.htm

[2] K. G. V. Seeberg, L. L. Andersen, E. Bengtsen, and E. Sundstrup, "Effectiveness of workplace interventions in rehabilitating musculoskeletal disorders and preventing its consequences among workers with physical and sedentary employment: Systematic review protocol," *Systematic Rev.*, vol. 8, no. 1, pp. 1–7, 2019.

[3] T. Butler and J. C. Gillette, "Used as PPE for injury prevention," *Professional Saf.*, vol. 64, no. 3, pp. 33–37, 2019. [Online]. Available: https://lib.dr.iastate.edu/kin_pubs/47

[4] D. M. Kelson, S. Kim, M. A. Nussbaum, and D. Srinivasan, "Effects of passive upper-extremity exoskeleton use on motor performance," *Proc. Human Factors Ergonom. Soc. Annu. Meeting*, vol. 63, pp. 1084–1085, 2019.

[5] P. Maurice *et al.*, "Human movement and ergonomics: An industry-oriented dataset for collaborative robotics," *Int. J. Robot. Res.*, vol. 38, no. 14, pp. 1529–1537, 2019.

[6] E. Rashedi, S. Kim, M. A. Nussbaum, and M. J. Agnew, "Ergonomic evaluation of a wearable assistive device for overhead work," *Ergonomics*, vol. 57, no. 12, pp. 1864–1874, 2014.

[7] D. Chiaradia, M. Xiloyannis, C. W. Antuvan, A. Frisoli, and L. Masia, "Design and embedded control of a soft elbow exosuit," in *Proc. IEEE Int. Conf. Soft Robot.*, 2018, pp. 565–571.

[8] B. K. Dinh, M. Xiloyannis, C. W. Antuvan, L. Cappello, and L. Masia, "Hierarchical cascade controller for assistance modulation in a soft wearable arm exoskeleton," *IEEE Robot. Automat. Lett.*, vol. 2, no. 3, pp. 1786–1793, Jul. 2017.

[9] C. O'Neill *et al.*, "Inflatable soft wearable robot for reducing therapist fatigue during upper extremity rehabilitation in severe stroke," *IEEE Robot. Automat. Lett.*, vol. 5, no. 3, pp. 3899–3906, Jul. 2020.

[10] C. S. Simpson, A. M. Okamura, and E. W. Hawkes, "Exomuscle: An inflatable device for shoulder abduction support," in *Proc. IEEE Int. Conf. Robot. Automat.*, 2017, pp. 6651–6657.

[11] S. Lessard, P. Pansodtee, A. Robbins, J. M. Trombadore, S. Kurniawan, and M. Teodorescu, "A soft exosuit for flexible upper-extremity rehabilitation," *IEEE Trans. Neural Syst. Rehabil. Eng.*, vol. 26, no. 8, pp. 1604–1617, Aug. 2018.

[12] K. Little *et al.*, "IMU-based assistance modulation in upper limb soft wearable exosuits," in *Proc. IEEE Internal Conf. Rehabil. Robot.*, 2019, pp. 1197–1202.

[13] D. H. Moon, D. Kim, and Y. D. Hong, "Development of a single leg knee exoskeleton and sensing knee center of rotation change for intention detection," *Sensors*, vol. 19, no. 18, 2019, Art. no. 3960.

[14] J. Bae *et al.*, "A lightweight and efficient portable soft exosuit for paretic ankle assistance in walking after stroke," in *Proc. IEEE Int. Conf. Robot. Automat.*, 2018, pp. 2820–2827.

[15] Z. Lu, X. Chen, X. Zhang, K. Y. Tong, and P. Zhou, "Real-time control of an exoskeleton hand robot with myoelectric pattern recognition," *Int. J. Neural Syst.*, vol. 27, no. 5, pp. 1–11, 2017.

[16] C. G. McDonald, T. A. Dennis, and M. K. O'Malley, "Characterization of surface electromyography patterns of healthy and incomplete spinal cord injury subjects interacting with an upper-extremity exoskeleton," in *IEEE Int. Conf. Rehabil. Robot.*, 2017, pp. 164–169.

[17] J. Rosen, M. Brand, M. B. Fuchs, and M. Arcan, "A myosignal-based powered exoskeleton system," *IEEE Trans. Syst., Man, Cybernetics Part A:Syst. Humans.*, vol. 31, no. 3, pp. 210–222, May 2001.

[18] A. W. Oyong, S. Parasuraman, and V. L. Jauw, "Robot assisted stroke rehabilitation: Estimation of muscle force/joint torque from EMG using GA," in *Proc. IEEE EMBS Conf. Biomed. Eng. Sci.*, 2010, pp. 341–347.

[19] A. Lince *et al.*, "Design and testing of an under-actuated surface EMG-driven hand exoskeleton," in *Proc. IEEE Int. Conf. Rehabil. Robot.*, 2017, pp. 670–675.

[20] R. D. Wilson *et al.*, "Upper-limb recovery after stroke: A randomized controlled trial comparing EMG-Triggered, cyclic, and sensory electrical stimulation," *Neurorehabilitation Neural Repair*, vol. 30, no. 10, pp. 978–987, 2016.

[21] R. Abbasi-Kesbi, H. Memarzadeh-Tehran, and M. J. Deen, "Technique to estimate human reaction time based on visual perception," *Healthcare Technol. Lett.*, vol. 4, no. 2, pp. 73–77, 2017.